WAVELET-BASED PARALLEL MRI REGULARIZATION USING BIVARIATE SPARSITY PROMOTING PRIORS

Lotfi Chaâri[1,3]*, Amel Benazza-Benyahia*[2]*, Jean-Christophe Pesquet*[1] *and Philippe Ciuciu*[3]

[1] Université Paris-Est, IGM and
UMR-CNRS 8049,
77454 Marne-la-Vallée cedex, France
{chaari,pesquet}@univ-mlv.fr

[2] URISA, SUP'COM
Cité Technologique des Communications,
2083, Tunisia
benazza.amel@supcom.rnu.tn

[3] CEA/DSV/I^{2}BM/Neurospin
CEA Saclay, Bbt. 145, Point Courrier 156,
91191 Gif-sur-Yvette cedex, France
philippe.ciuciu@cea.fr

ABSTRACT

Parallel magnetic resonance imaging (pMRI) using multiple receiver coils has emerged as a powerful 3D imaging technique for reducing scanning time or increasing image resolution. The acquired k-space is subsampled, and full Field of View (FoV) images are then reconstructed from the acquired aliased data, by applying methods such as the widely-used SENSE algorithm. However, reconstructed images using SENSE may suffer from several kinds of artifacts mainly because of the noise and inaccurate sensitivity profiles. In this paper, we propose an appproach for regularized SENSE reconstruction in the wavelet transform domain. More precisely, a Bayesian strategy is adopted by introducing a bivariate prior to model the complex-valued signal. Experiments on synthetic data and real T1-weighted MRI images at 1.5 Tesla magnetic field show that the proposed method reduces reconstruction artifacts.

***Index Terms*—** MRI, regularization, sparsity, wavelets, bivariate prior, Bayesian approaches, convex optimization.

1. INTRODUCTION

Since the early 1990's, parallel Magnetic Resonance Imaging (MRI) has been recognized as a fast efficient MRI technique. Several data sets are sampled at a rate R times lower than the Nyquist one along the phase encoding direction. These data are simultaneously acquired by multiple coils surrounding the object under investigation with different geometric orientations. The subsampling rate entails an acquisition duration R times shorter than that required by conventional MRI. This is of particular interest for tracking fast biological phenomena such as blood flow changes in the brain that accompany increases in neural activity. However, because of the sub-sampling, only reduced FoV images are acquired in each coil. The recovery of the full FoV image is achieved using both all coil images and sensitivity profiles. This constitutes a difficult task as the collected data are often corrupted by both aliasing distortions and observation noise. Furthermore, when the coil sensitivity map is required as a prior knowledge, its inaccurate estimation may yield to a poor reconstruction performance. In this regard, several reconstruction methods have been reported [1, 2]. The pioneering reconstruction method SMASH (Simultaneous Acquisition of Spatial Harmonics) proposed by Sodickson and Manning in 1997 [1], operates in the k-space domain. A linear combination of coil sensitivity maps is then used to recover the missing phase encoding steps. However, these k-space based methods do not always provide satisfactory results at low acquisition signal-to-noise ratio (SNR). The SENSE (Sensitivity Encoding) technique has been proposed in [2] as an alternative, which relies on a weighted least squares estimation procedure in the image domain. The considered inverse problem being ill-conditioned, two kinds of solutions have been investigated. The first one aims at optimizing the coil geometry [3] or/and at improving the estimation of the sensitivity maps [4, 5]. The second class of solutions consists of resorting to regularization techniques [6, 7]. Indeed, it has been found that regularization tools allow us to obtain a significant enhancement of the reconstructed image quality even at high reduction factors (e.g. $R = 4$) and low magnetic field (1.5 Tesla). In a previous work [7], we have proposed a new regularized technique which considers a sparse representation of the data and performs an efficient reconstruction within a Bayesian framework. Under severe experimental conditions, this method outperforms the SENSE regularized methods. In this paper, we aim at improving the performance of our method. Our contribution is twofold. First, it consists of designing more realistic (and hence, more accurate) sparse prior distributions for the wavelet coefficients of the sought image. Second, we apply a fast optimization procedure of the resulting regularization criterion. The remainder of this paper is organized as follows. In Section 2, we briefly introduce the context of our work. In Section 3, we study the statistics of the complex-valued wavelet coefficient of MRI slices to deduce a novel bivariate model that we validate. In Section 4, we describe the proposed regularization method. Experimental results obtained on synthetic and real data are provided in Section 5. Finally, some conclusions and perspectives are drawn in Section 6.

This work was supported by grants from Région Ile de France and the Agence Nationale de la Recherche under grant ANR-05-MMSA-0014-01.

2. PARALLEL MRI

Although parallel MRI is a 3D imaging technique, it proceeds with a slice by slice acquisition to get all the 3D volume, which simplifies the problem to a two-dimensional one. In what follows, we are only interested in reconstructing a given slice (2D image).

2.1. Observation model

An array of L coils is used to measure the spin density $\overline{\rho}$ of the subject under investigation. The signal $\widetilde{d}_l$ received by each coil l ($1 \leq l \leq L$) is evaluated at location $\boldsymbol{k} = (k_x, k_y)^{\mathsf{T}}$ in the frequency space (k-space). Ideally, it corresponds to the Fourier transform of the desired 2D field $\overline{\rho}$ weighted by the coil sensitivity profile s_l. In practice, it is corrupted by a zero-mean additive Gaussian noise n_l:

$$\widetilde{d}_l(\boldsymbol{k}) = \int \overline{\rho}(\boldsymbol{r}) s_l(\boldsymbol{r}) e^{-\imath 2\pi \boldsymbol{k}^{\mathsf{T}}\boldsymbol{r}} d\boldsymbol{r} + n_l(\boldsymbol{k}) \qquad (1)$$

where $\boldsymbol{r} = (x, y)^{\mathsf{T}}$ is the spatial position in the image domain. Generally, the sampling of $\widetilde{d}_l$ in brain imaging is performed according to a Cartesian rectangular grid due to its simplicity. In its simplest form,

and due to the separability of the Fourier transform, SENSE imaging amounts to an inversion problem along a single direction (namely the phase encoding direction or the x-axis). In parallel MRI, a reduction factor $R \leq L$ is considered in order to only register one line over R, the sampling period being $\Delta x = \frac{X}{R}$ where X is the size of $\overline{\rho}$ along the x-axis. Consequently, Eq. (1) becomes:

$$\boldsymbol{d}(\boldsymbol{r}) = \boldsymbol{S}(\boldsymbol{r})\overline{\boldsymbol{\rho}}(\boldsymbol{r}) + \boldsymbol{n}(\boldsymbol{r}) \tag{2}$$

$$\text{where } \boldsymbol{S}(\boldsymbol{r}) \triangleq \begin{bmatrix} s_1(x,y) & \dots & s_1(x+(R-1)\Delta x, y) \\ \vdots & \dots & \vdots \\ s_L(x,y) & \dots & s_L(x+(R-1)\Delta x, y) \end{bmatrix},$$

$$\boldsymbol{d}(\boldsymbol{r}) \triangleq [d_1(x,y), \dots, d_L(x,y)]^{\mathsf{T}}, \boldsymbol{n}(\boldsymbol{r}) \triangleq [n_1(x,y), \dots, n_L(x,y)]^{\mathsf{T}}$$

$$\overline{\boldsymbol{\rho}}(\boldsymbol{r}) \triangleq [\overline{\rho}(x,y), \dots, \overline{\rho}(x+(R-1)\Delta x, y)]^{\mathsf{T}},$$

and d_l denotes the inverse Fourier transform of $\widetilde{d}_l$ with $l \in \{1, \dots, L\}$. It can be assumed that $(\boldsymbol{n}(\boldsymbol{r}))_{\boldsymbol{r}}$ is a sequence of circular Gaussian complex-valued random vectors, which are spatially independent, with zero-mean and an invertible covariance matrix $\boldsymbol{\Psi}$. The objective is to obtain an estimate $\widehat{\boldsymbol{\rho}}(\boldsymbol{r})$ of $\overline{\boldsymbol{\rho}}(\boldsymbol{r})$ from $\boldsymbol{d}(\boldsymbol{r})$ at each spatial position $\boldsymbol{r}$.

2.2. Basic SENSE method

The weighted least squares criterion is minimized in the SENSE method by using $\boldsymbol{\Psi}^{-1}$ as the weighting matrix, which must also be estimated. This results in the following classical estimate:

$$\widehat{\boldsymbol{\rho}}_{\mathrm{WLS}}(\boldsymbol{r}) = [\boldsymbol{S}^{\mathsf{H}}(\boldsymbol{r})\boldsymbol{\Psi}^{-1}\boldsymbol{S}(\boldsymbol{r})]^{-1}\boldsymbol{S}^{\mathsf{H}}(\boldsymbol{r})\boldsymbol{\Psi}^{-1}\boldsymbol{d}(\boldsymbol{r}) \tag{3}$$

where $(\cdot)^{\mathsf{H}}$ stands for the transposed complex conjugate. In practice, if the matrix $\boldsymbol{S}^{\mathsf{H}}(\boldsymbol{r})\boldsymbol{\Psi}^{-1}\boldsymbol{S}(\boldsymbol{r})$ is ill-conditioned, the quality of the reconstructed image is altered. As shown in Fig. 1, at high reduction factors like $R = 4$, aliasing artifacts in $\widehat{\rho}_{\mathrm{WLS}}$ are clearly visible. One possible solution to circumvent this drawback is to resort to regularization [8, 9]. In [7], we have proposed to carry out the regularization on the Wavelet Transform (WT) coefficients of the FoV image. In the next section, we study the wavelet coefficient statistics in more details and emphasize our contributions.

3. STATISTICAL STUDY AND OPTIMIZATION TOOLS

3.1. Notations

Let T denote the dyadic WT operator. It is associated with a discrete decomposition onto a separable 2D orthogonal wavelet basis performed over J resolution levels [10]. The operator T is applied to the target image ρ of size $X \times Y$ and a complex-valued coefficient field $\zeta = \big((\zeta_{a,k})_{1\leq k\leq K_J}, (\zeta_{o,j,k})_{1\leq j\leq J, 1\leq k\leq K_j}\big)$ is generated where $K_j = XY/4^j$ is the number of wavelet coefficients in a given subband at resolution j. The coefficients have been reindexed in such a way that $\zeta_{a,k}$ corresponds to an approximation coefficient at the coarsest resolution level J and spatial position k, $\zeta_{o,j,k}$ is a wavelet coefficient oriented either horizontally ($o = 1$), vertically ($o = 2$) or diagonally ($o = 3$) at resolution level j and position k. The principle of our approach consists of computing a Bayesian estimate $\widehat{\zeta}$ of the field of wavelet coefficients. Then, an inverse WT is applied to $\widehat{\zeta}$ in order to recover the reconstructed FoV image.

3.2. Prior selection

In this context, a key issue is the selection of a prior model for the wavelet coefficients at each resolution level and orientation. As the latter coefficients are complex-valued, a simple approach is to assume that their real and imaginary parts are mutually independent. In [7], independent Generalized Gaussian (GG) priors have been used in order to separately model the distributions of the real and the imaginary parts of the wavelet coefficients of the sought image. The related hyperparameters were estimated using the maximum likelihood criterion. Despite its simplicity, this model does not account for the statistical dependence between the real and imaginary parts. In fact, kernel statistical tests of independence [11] applied on our experimental data sets indicate that the hypothesis "the real and imaginary parts are independent" is rejected with an error level less than 2%. In this paper, we provide a more accurate modelling by considering the *joint* distribution of the two parts through an appropriate bivariate prior probability density function (PDF). From the examination of the joint empirical histograms, it seems more appropriate to consider the following PDF form:

$$\forall \xi \in \mathbb{C}, \quad f_{\alpha,\beta,\gamma,p}(\xi) = Ce^{-(\alpha|\mathrm{Re}(\xi)|+\beta|\mathrm{Im}(\xi)|+\gamma|\xi|^p)} \tag{4}$$

where $C \in \mathbb{R}_+^*$ is a normalization constant, and where the hyperparameters α, β, γ belong to $\mathbb{R}_+^*$ and $p \in [1, \infty[$. It can be noticed that the proposed class of PDFs includes those considered in [12] for denoising purposes as particular cases when $\alpha = \beta$ and $p = 1$.
Note also that a less general model has been used in our previous work [13] to model jointly real and imaginary parts of the wavelet coefficients. This model may be derived from the one adopted in this paper by setting $\alpha = \beta = 0$. In practice, the hyperparameters have been estimated using a Markov Chain Monte Carlo (MCMC) [14] procedure since the maximum likelihood estimator does not have a tractable expression, as the constant C_f cannot be derived analytically. For illustration, Fig. 2 shows the empirical histogram of the coefficients $(\zeta_{1,2,k})_k$, the independent PDF used in [7] and the adopted bivariate PDF in (4). It is clear that, due to the elliptical shape, the bivariate model better fits the empirical histogram than the independent one. For instance, according to the independent model, some pairs of values of $(\mathrm{Re}(\zeta_{1,2,k}), \mathrm{Im}(\zeta_{1,2,k}))$ have an over/under-estimated occurrence frequency w.r.t. the empirical joint histogram and the bivariate model.

3.3. Bivariate proximal thresholding

A fundamental tool in modern convex optimization is the concept of proximity operator [15]. We recall that, in a given separable complex Hilbert space χ, the proximity operator of any lower semicontinuous convex function Φ from χ to $]-\infty, +\infty]$, denoted by prox_Φ , is defined as

$$\forall \mathsf{x} \in \chi, \quad \mathrm{prox}_\Phi(\mathsf{x}) = \arg\min_{\mathsf{y}\in\chi} \frac{1}{2}\|\mathsf{y}-\mathsf{x}\|^2 + \Phi(\mathsf{y}). \tag{5}$$

As shown below, it is possible to give a closed form expression of the proximity operator of the potential function associated with the proposed bivariate PDF:

$$\forall \xi \in \mathbb{C}, \quad \Phi(\xi) = \alpha|\mathrm{Re}(\xi)| + \beta|\mathrm{Im}(\xi)| + \gamma|\xi|^p. \tag{6}$$

Proposition 3.1 *We have, for every $\xi \in \mathbb{C}$,*

$$\mathrm{prox}_\Phi(\xi) = \mathrm{prox}_\varphi\Big(\mathrm{soft}_\alpha(\mathrm{Re}(\xi)) + \imath\, \mathrm{soft}_\beta(\mathrm{Im}(\xi))\Big) \tag{7}$$

where soft_τ with $\tau \geq 0$ is the real-valued soft-thresholding operator defined by: $\forall \xi \in \mathbb{R}, \mathrm{soft}_\tau(\xi) = \mathrm{sign}(\xi)\max\{|\xi|-\tau, 0\}$ and prox_φ is the proximity operator of $\varphi = \gamma|\cdot|^p$ which is given by:

- *if* $p = 1$,

$$\forall \xi \in \mathbb{C}, \quad \mathrm{prox}_{\varphi}(\xi) = \begin{cases} \Big(1 - \dfrac{\gamma}{|\xi|}\Big)\xi & \text{if } |\xi| > \gamma \\ 0 & \text{otherwise} \end{cases} \tag{8}$$

- *if* $p > 1$,

$$\forall \xi \in \mathbb{C}, \quad \mathrm{prox}_{\varphi}(\xi) = \begin{cases} \Big(1 - \dfrac{\nu(\xi)}{|\xi|}\Big)\xi & \text{if } \xi \neq 0 \\ 0 & \text{otherwise} \end{cases} \tag{9}$$

where $\nu(\xi)$ *is the unique non-negative real solution of the equation* $\nu(\xi) + \big(\nu(\xi)/(\gamma p)\big)^{1/(p-1)} = |\xi|$.

This result constitutes a generalization to the complex case of [16, Prop. 3.6]. As a consequence, for every $\xi \in \mathbb{C}$ such that $(\mathrm{Re}(\xi), \mathrm{Im}(\xi)) \in [-\alpha, \alpha] \times [-\beta, \beta]$, $\mathrm{prox}_{\Phi}(\xi) = 0$, which means that prox_{Φ} is a bivariate *proximal thresholder* [16]. This shows that the proposed prior distribution should be helpful in promoting the sparsity of the wavelet representation of complex-valued data. Note here that the proximity operator corresponding to the less general prior in [13] can be derived as a particular case of the one given hereabove.

4. PROPOSED WAVELET-BASED REGULARIZATION

4.1. Principle

The field of wavelet coefficients will be estimated according to the Maximum A Posteriori (MAP) criterion based on the observation $\boldsymbol{d}$. The advantage of considering the WT is twofold. Indeed, when carefully inspecting the SENSE-based reconstructed images $\widehat{\rho}_{\mathrm{WLS}}$ (see Fig. 1), artifacts correspond to distorted curves with either very high or very low intensity, spatially-localized. Therefore, our rationale is to use an image representation which facilitates the detection of these undesirable aliasing structures so as to attenuate them in the reconstruction process. In this respect, the WT has been recognized as an efficient tool [10]. Besides, the estimation procedure can be easily conducted within the Bayesian framework since the WT allows us to design tractable prior distributions for the coefficient field as discussed in the previous section.

4.2. Problem formulation

The MAP estimation of the wavelet coefficients consists of computing an estimate $\widehat{\zeta}$ such that

$$\widehat{\zeta} = \arg\max_{\zeta} \big[\ln f(\zeta) + \ln g(\boldsymbol{d} \mid T^{-1}\zeta) \big] \tag{10}$$

where f is the prior PDF of ζ and g stands for the likelihood of the observed data. Since the additive noise occuring during the acquisition process is an i.i.d complex-valued circular Gaussian noise, g can be expressed as:

$$g(\boldsymbol{d} \mid \rho) \propto \exp\left(-G(\rho)\right) \tag{11}$$

where $G(\rho) = \sum_{\boldsymbol{r}} \parallel \boldsymbol{d}(\boldsymbol{r}) - \boldsymbol{S}(\boldsymbol{r})\boldsymbol{\rho}(\boldsymbol{r}) \parallel^2_{\boldsymbol{\Psi}^{-1}}$ and $\| \cdot \|_{\boldsymbol{\Psi}^{-1}} = \sqrt{(\cdot)^{\mathsf{H}} \boldsymbol{\Psi}^{-1} (\cdot)}$. We recall that $\rho = T^{-1}\zeta$.

4.3. Iterative optimization procedure

Combining equations (4) and (10) and assuming the independence of the complex-valued wavelet coefficients leads to minimizing

$$\mathcal{C}(\zeta) = G(T^{-1}\zeta) + \sum_{k=1}^{K_J} \Phi_a(\zeta_{a,k}) + \sum_{j=1}^{J} \sum_{o=1}^{3} \sum_{k=1}^{K_j} \Phi_{o,j}(\zeta_{o,j,k}),$$

where

$$\Phi_{o,j}(\zeta_{o,j,k}) = \alpha_{o,j}|\mathrm{Re}(\zeta_{o,j,k})| + \beta_{o,j}|\mathrm{Im}(\zeta_{o,j,k})| + \gamma_{o,j}|\zeta_{o,j,k}|^{p_{o,j}}$$

and Φ_a is similarly defined (once the approximation have been centered). Although G is differentiable with a continuous Lipschitz-gradient ∇G, the resulting criterion $\mathcal{C}$ is not differentiable and its minimum cannot be explicitly derived. A forward-backward minimization procedure [17] is then employed whose main steps are outlined in Algorithm 1. The computation of the proximity operators involved in this algorithm is derived from Proposition 3.1.

Algorithm 1 forward-backward

1: Initialize ζ, fix the relaxation parameter $\lambda \in]0, 1]$, compute the Lipschitz constant κ of the gradient ∇G and fix the step-size parameter $\gamma \in]0, \frac{2}{\kappa}[$.
2: **while** $|\frac{\mathcal{C}^{(n)} - \mathcal{C}^{(n-1)}}{\mathcal{C}^{(n-1)}}| > \varepsilon$ **do**
3: $\quad \zeta_{o,j,k} \leftarrow \zeta_{o,j,k} + \lambda\Big(\mathrm{prox}_{\gamma\Phi_{o,j}}(\zeta_{o,j,k} - \gamma[\nabla G(T^{-1}\zeta)]_{o,j,k}) - \zeta_{o,j,k}\Big)$ (at each iteration n, update $\zeta_{a,k}$ similarly)
4: **end while**
5: **return** ζ

5. EXPERIMENTAL RESULTS

5.1. Synthetic data

A first set of experiments was carried out on synthetic data. The complex-valued observations have been generated according to the SENSE acquisition model in (2) from a known reference image ρ_{ref}, using $L = 8$ coils and i.i.d circular Gaussian noise with zero-mean and variance σ^2. Data have been simulated using $\boldsymbol{\Psi} = \sigma^2 \boldsymbol{I}_8$ for different values of σ^2 where $\boldsymbol{I}_8$ is the 8×8 identity matrix. We have used the Symmlet 8 wavelet basis over $J = 3$ resolution levels. In order to validate the choice of the bivariate prior, we have resorted to the Kolmogorov-Smirnov test of fit. It indicates a valid prior bivariate model for almost all subbands. Table 1 gives the values of the resulting signal-to-noise ratios $\mathrm{SNR} = 20\log_{10}\big(\frac{\|\rho_{\mathrm{ref}}\|_2}{\|\rho_{\mathrm{ref}} - \widehat{\rho}\|_2}\big)$ of the reconstructed image $\widehat{\rho}$ for the univariate and the bivariate prior models at different noise levels. SNR values indicate that the best accuracy of the reconstruction process is achieved by the bivariate model for which significant quantitative improvements are obtained w.r.t the univariate model and the SENSE approach. This corroborates the fact that the real and imaginary parts are statistically dependent.

5.2. Real data

The second round of experiments was conducted on T1-weighted anatomical images of in-plane dimension 256$\times$ 256 and 0.93$\times$ 0.93$\times$ 8 (mm) spatial resolution. A Signa 1.5 Tesla GE Healthcare scanner has been used with $L = 8$ head-coils. The reduction factor $R = 4$ can be considered as high for such a low magnetic field. We kept the same wavelet basis and prior models as in the experiments on synthetic data. The Kolmogorov-Smirnov test of fit was also used to validate the matching of the proposed model. Fig. 3 illustrates an example of reconstructed images (a zoom) using WT regularization with the independent (middle) and the proposed bivariate (right) models, in addition to the SENSE-based reconstruction (left). We can notice that aliasing artifacts appearing in the SENSE-based reconstructed image are considerably smoothed. Comparing with the independent model, the proposed method gives a better reconstruction quality: some of the aliasing artifacts are better smoothed when the bivariate model is used. Table 2 gives the SNR values for three reconstructed slices and shows that the reconstruction quality is improved with the bivariate model when compared with SENSE

and the independent one. Note that SNR values have been computed using a reference image reconstructed with a non accelerated acquisition ($R = 1$). After this SNR statistical analysis, we need to mention that it is pretty difficult to state a clear correspondance between the SNR improvment and the artifact removal. Note that the real MRI dataset, which has been acquired at 1.5 Tesla, is made up of a single volume. However, on the same scanner at 1.5 Tesla, we have also validated our approach on functional MRI data. The fMRI dataset is composed of 30 volumes acquired every 2.4 seconds each and has been acquired during resting-state (subject lying on the bed with eyes closed), which means with no external stimulation. BOLD signal analysis showed that the proposed approach gives almost constant signal, in contrast to SENSE or Tikhonov reconstruction.

6. CONCLUSION

In this paper, we have proposed a wavelet-based method for image reconstruction in parallel MRI through an efficient Bayesian framework based on a suitable bivariate prior. The proposed approach can be extended to functional MRI data reconstruction to enhance activation detection for high reduction factors. It can also be applied to other image regularization problems dealing with complex-valued data.

7. REFERENCES

[1] D. K. Sodickson and W. J. Manning, "Simultaneous acquisition of spatial harmonics (SMASH): fast imaging with radiofrequency coil arrays," *Magn. Res. Med.*, vol. 38, no. 4, pp. 591–603, June 1999.

[2] K. P. Pruessmann, M. Weiger, M. B. Scheidegger, and P. Boesiger, "SENSE: sensitivity encoding for fast MRI," *Magn. Res. Med.*, vol. 42, no. 5, pp. 952–962, Jul. 1999.

[3] M. Weiger, K. P. Pruessmann, C. Lessler, P. Roschmann, and P. Boeisiger, "Specific coil design for SENSE: a six-element cardiac array," *Magn. Res. Med.*, vol. 45, no. 3, pp. 495–504, Feb. 2001.

[4] Q. M. Tieng, V. Vegh, G. J Cowin, and Z. Yang, "Fast parallel image reconstruction using SMACKER for functional magnetic resonance imaging," in *IEEE ISBI*, Paris, May 14-17 2008, pp. 564–567.

[5] W. S. Hoge and D. H. Brooks, "Using GRAPPA to improve autocalibrated coil sensitivity estimation for the SENSE family of parallel imaging reconstruction algorithms," *Magnetic Resonance in Medicine*, vol. 60, no. 2, pp. 462–467, Jul. 2008.

[6] B. Liu, L. Ying, M. Steckner, X. Jun, and J. Sheng, "Regularized SENSE reconstruction using iteratively refined total variation method," in *IEEE ISBI*, Washington DC, Apr. 12-15 2007, pp. 121 – 124.

[7] L. Chaâri, J.-C. Pesquet, A. Benazza-Benyahia, and Ph. Ciuciu, "Autocalibrated parallel MRI reconstruction in the wavelet domain," in *IEEE ISBI*, Paris, May 14-17 2008, pp. 756–759.

[8] L. Ying, D. Xu, and Z.-P. Liang, "On Tikhonov Regularization for image reconstruction in parallel MRI," in *IEEE EMBS*, San Francisco, Sept. 1-5 2004, pp. 1056–1059.

[9] B. Liu, K. King, M. Steckner, J. Xie, J. Sheng, and L. Ying, "Regularized sensitivity encoding (SENSE) reconstruction using bregman iterations," *Magn. Res. Med.*, vol. 61, no. 1, pp. 145 – 152, Dec. 2008.

[10] S. Mallat, *A wavelet tour of signal processing*, Academic Press, New York, 1999.

[11] A. Gretton, K. Fukumizu, C. H. Teo, L. Song, B. Schlkopf, and A. J. Smola, "A kernel statistical test of independence," in *Advances in Neural Information Processing Systems*, 2007, pp. 585–592.

[12] L. Sendur and I. W. Selesnick, "Bivariate shrinkage functions for wavelet-based denoising exploiting interscale dependency," *IEEE Trans. Sig. Proc.*, vol. 50, no. 11, pp. 2744–2756, Nov. 2002.

[13] L. Chaâri, J.-C. Pesquet, A. Benazza-Benyahia, and Ph. Ciuciu, "Minimization of a sparsity promoting criterion for the recovery of complex-valued signals," in *SPARS*, Saint-Malo, France, Apr. 06-09 2009, 4 pp.

[14] C. Robert and G. Castella, *Monte Carlo statistical methods*, Springer, New York, 2004.

[15] P. L. Combettes and V. R. Wajs, "Signal recovery by proximal forward-backward splitting," *Mult. Model. Simul.*, vol. 4, pp. 1168–1200, Nov. 2005.

[16] P. L. Combettes and J.-C. Pesquet, "Proximal thresholding algorithm for minimization over orthonormal bases," *SIAM Jour. Opt.*, vol. 18, pp. 1351–1376, Oct. 2007.

[17] C. Chaux, P. Combettes, J.-C. Pesquet, and V.R Wajs, "A variational formulation for frame-based inverse problems," *Inv. Prob.*, vol. 23, no. 4, pp. 1495–1518, Aug. 2007.

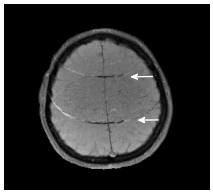

Fig. 1. Aliasing artefacts in the reconstructed image using the basic SENSE algorithm with $R = 4$.

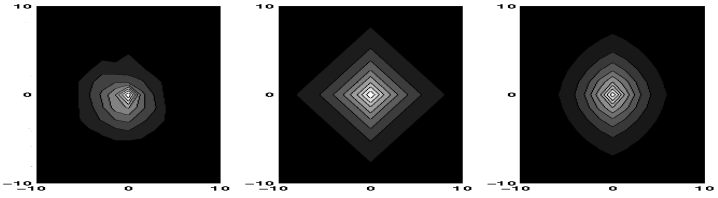

Fig. 2. Joint 2D empirical histogram $(\zeta_{1,2,k})_k$ (left) and PDFs of the independent (middle) and bivariate (right) models.

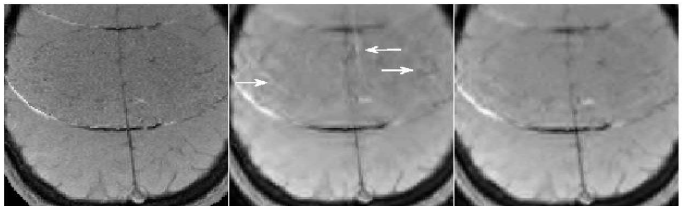

Fig. 3. Reconstructed images using SENSE (left) and the WT regularization with the independent model (middle) and the proposed bivariate one (right) for $R = 4$.

Table 1. SNR (dB) evaluation for synthetic data.

σ \ SNR	SENSE	Independent model	Bivariate model
8	17.68	21.10	21.27
14	12.77	19.08	19.45
20	9.80	17.40	17.77

Table 2. SNR (dB) evaluation for real data.

	SENSE	Independent model	Bivariate model
Slice 1	14.15	14.30	14.62
Slice 2	12.19	12.90	13.15
Slice 3	11.49	12.06	12.40